energies

MDPI

Article

Mechanical Behavior and Permeability Evolution of Reconstituted Coal Samples under Various Unloading Confining Pressures—Implications for Wellbore Stability Analysis

Qiangui Zhang [1,2,3], Xiangyu Fan [2,3], Yongchang Liang [3], Minghui Li [1], Guangzhi Li [1], Tianshou Ma [2,3] and Wen Nie [4,5,*]

1 State Key Laboratory of Coal Mine Disaster Dynamics and Control, Chongqing University, Chongqing 400030, China; qgzhang@swpu.edu.cn (Q.Z.); cqumhli@vip.163.com (M.L.); lgz@cqu.edu.cn (G.L.)
2 State Key Laboratory of Oil and Gas Reservoir Geology and Exploitation, Southwest Petroleum University, Chengdu 610500, China; fanxy666@swpu.edu.cn (X.F.); matianshou@126.com (T.M.)
3 College of Petroleum Engineering, Southwest Petroleum University, Chengdu 610500, China; lychcqu@163.com
4 Quanzhou Institute of Equipment Manufacturing, Haixi Institutes, Chinese Academy of Sciences, Quanzhou 362200, China
5 Landslide Research, Faculty of Civil Geo and Environmental Engineering, Technische Universität München, 80333 Munich, Germany
* Correspondence: niewen1026@gmail.com; Tel.: +49-0176-3119-9092

Academic Editor: Mofazzal Hossain
Received: 14 December 2016; Accepted: 28 February 2017; Published: 2 March 2017

Abstract: Low pressure, low permeability, and low saturation of Chinese coal-bed methane (CBM) reservoirs make underbalanced drilling (UBD) widely used for mining CBM in China. In this study, mechanical behavior and permeability of coal rock were investigated under different degrees of unloading confining pressure (UCP)-reloading axial stress (RAS) by a triaxial experimental apparatus. These tests revealed that: (1) peak deviatoric stress of coal rock in UCP-RAS is lower than that in a conventional triaxial compression (CTC) test, and the peak deviatoric stress linearly relates the degree of unloading confining pressure. The deformation modulus of coal in UCP-RAS is lower than that in CTC, while the lateral expansion ratio is larger than that in CTC; (2) higher UCP leads to a faster increase of permeability during RAS until the failure of coal; (3) the cohesion and internal friction angle tested by UCP-RAS are lower by 4.57% and 15.18% than those tested by CTC. In addition, a field case (Zhaozhuang well, Qinshui Basin, China) of a well collapse problem validates the higher probability of wellbore collapse due to the increase of equivalent collapse fluid density, which is calculated by using coal rock parameters tested by UCP-RAS rather than by CTC.

Keywords: coal; coalbed methane; permeability; underbalanced drilling; unloading confining pressure

1. Introduction

Underbalanced drilling (UBD), which can avoid drilling fluid polluting reservoirs, is widely used for mining coal-bed methane (CBM) in China, considering the low pressure, low permeability, and low saturation of Chinese CBM reservoirs [1]. Compared to conventional overbalanced drilling (OBD), the bottom hole pressure (BHP) of UBD must reduce to a design value for lowering the formation pressure. The decrease of BHP can increase deviatoric stress on a coal wellbore [2] resulting in a lack of

effective support from drilling fluid [3], which is similar with an unloading confining pressure (UCP) in a triaxial stress condition. The UCP damages the coal mechanical property [4]. In addition, the permeability of the gas reservoir increased by the UCP [5] results in the damage of the mechanical behavior of coal [6]. Both aspects above threaten the coal wellbore stability [7].

The effect of UCP on the mechanical behavior of rocks is usually investigated by triaxial compression tests [8]. Damage to the mechanical behavior of rock under unloading conditions is of importance in the analysis of stress-induced failure of overstressed rock masses [9]. Xie and He [10] show that the rock strength under unloading conditions is lower than that under loading conditions. A higher UCP rate corresponds to lower compressive strength and ductile strain [11]. The failure mode of the rock specimen gradually changes from shear to tensile with the increasing UCP rate [12]. The radial deformation produced by unloading is often more than the axial deformation [13]. These investigations reveal that the mechanical characteristics of rocks reduce under UCP and the increased UCP rate easily induces failure of rocks.

The deformation under UCP also influences the permeability of rocks [14]. The radial strain is a key variable for the evolution of permeability and the effect of UCP on the permeability cannot be ignored [4]. UCP causes an obvious expansion of the rock volume, which leads to high rock penetrability under unloading than that under loading conditions [15]. The UCP condition increases coal permeability much earlier than that under constant confining pressure [11]. During the unloading stage, the rock permeability shows a positive exponential relationship with the axial strain of the rock [16]. Rock penetrability induced by UCP is small at the initial elastic deformation phase, but increases near the end of the elastic deformation phase [17]. These investigations show that the permeability of rocks significantly and quickly increases during the UCP process.

However, all of the above studies did not consider the in situ conditions during CBM well transforming from conventional drilling methods to UBD. In the present work, considering this field status, the mechanical behavior and permeability of coal after suffering different degrees of UCP were investigated by a triaxial experimental apparatus. In addition, the equivalent collapse fluid densities (minimum drilling fluid density maintaining coal wellbore stability) calculated by using parameters from CTC and UCP-RAS tests were compared for evaluating the stability of a field coal wellbore case (Zhaozhuang well, Qinshui Basin, China).

2. Experimental Procedures

2.1. Experimental Apparatuses

"THM coupled with triaxial servo-controlled seepage apparatus for gas infiltrated coal" [18] is used for our experiments (Figure 1). The device includes a servo loading system, pressure chamber, constant temperature oil heating system, gas pressure control system, data acquisition and storage system, and auxiliary system. The technical specifications of this apparatus are as shown in Table 1. This apparatus is applicable to investigate the combined effect of stress, strain, temperature, and gas flow on the mechanical behavior and permeability of coal specimens [19].

Table 1. Technical specification of the apparatus.

Maximum Axial Stress	Maximum Confining Pressure	Frame Stiffness	Maximum Gas Pressure	Maximum Axial Displacement	Maximum Circumference Deformation
100 MPa	10 MPa	10 GN/m	6 MPa	60 mm	6 mm
Temperature Range	**Control Precision of Stress**	**Test Precision of Stress**	**Test Precision of Deformation**	**Control Precision of Temperature**	**Test Precision of Permeability**
Indoor temperature −100 °C	±0.5% of indicating value	±1% of indicating value	±1% of indicating value	±0.1 °C	±1% of indicating value

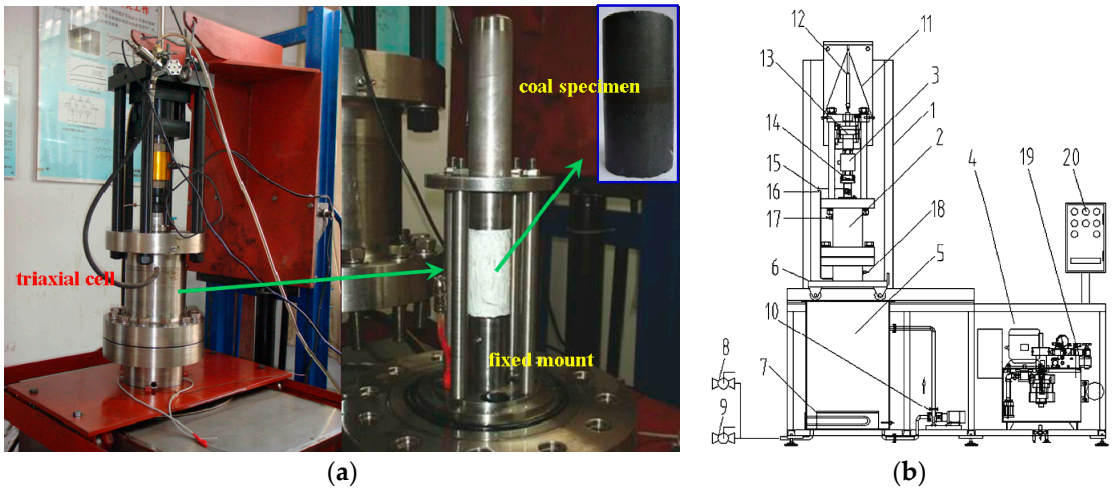

(**a**) (**b**)

Figure 1. Apparatus and specimen installation: (**a**) photo of the apparatus; (**b**) schematic of the apparatus. 1. Lifter; 2. triaxial chamber; 3. sensor of axial stress; 4. servo-controlled hydraulic pump; 5. water tank; 6. movable work platform; 7. heater tubes; 8. water inlet valve; 9. water drain valve; 10. water circulating pump; 11. lifting rope; 12. sensor of axial displacement; 13. hydraulic cylinder of axial stress; 14. force plate; 15. gas inlet valve; 16. gas outlet valve; 17. air drain valve; 18. hydraulic oil inlet/drain valve; 19. servo valve; 20. controlling stand.

2.2. Specimen Preparations and Basic Parameters

The coal samples were taken from the third coal seam of the Zhaozhuang coal mine of the Qinshui coalfield in Jincheng, Shanxi Province, China. This is an advanced industrial district of CBM exploration. These coal blocks are soft and fragile and their physical and mechanical parameters are as shown in Table 2. The data of density, BET surface area, and porosity were measured by the rock pieces experiment, and the data of the elasticity modulus, Poisson's ratio, and Boit coefficient were obtained by the logging analysis of a test horizontal well introduced in Section 4. The vertical depth of coal blocks from the coal seam of the test CBM horizontal well is about 720 m in a coal mine. In this seam, the high deviation of the horizontal in situ stress gradient (0.75 MPa) could potentially produce extreme fracture development in coal. Additionally, the process of taking coal blocks also could cause a stress release resulting in more fragmentation of the coal. These conditions make it difficult to obtain an intact coal rock. Therefore, we used the reconstituted coal samples in experiments.

Table 2. Characterization data of coal blocks.

Density (g/cm^3)	BET Surface Area (m^2/g)	Porosity (%)
$\frac{1.192-1.297}{1.236} \times 12$	$\frac{2.35-2.87}{2.63} \times 9$	$\frac{0.087-0.14}{0.10} \times 9$
Elasticity Modulus (GPa)	**Poisson's Ratio**	**Boit Coefficient**
$\frac{0.57-1.15}{0.83} \times 6$	$\frac{0.18-0.33}{0.26} \times 6$	$\frac{0.43-0.62}{0.53} \times 6$

The symbolic model of the number is $\frac{\text{Minimum value}-\text{Maximun value}}{\text{Average value}} \times$ sample amount.

The reconstituted coal specimens are used for our experiments. The coal powder has a particle size of 0.250–0.425 mm, and this particle size of coal powder was shaped by mixing with water for a 3% moisture content. The reconstituted coal specimens are shaped into a diameter of 50 mm and a height 100 mm $\pm$ 0.25 mm, with a pressure of 100 MPa by an implosion sampling machine. This pressure is according to the "general requirements for sampling (China National Code of GB/T 23561.1-2009)". The numbers, sizes, and densities of the coal specimens are as shown in Table 3.

2.3. Experimental Schemes

The experimental scheme is determined according to the stress state of the wellbore during UBD introduced here. During UBD, considering the gas flowing along the radial direction, the stress state of a cylindrical micro-unit of the well wall (Figure 2) can be expressed as [20]:

$$\begin{cases} \sigma_r = p_i - \phi(p_i - p_p) \\ \sigma_\theta = A\sigma_h + B\sigma_H + C\sigma_v + (K_1 - 1)p_i - K_1 p_p \\ \sigma_z = D\sigma_h + E\sigma_H + F\sigma_v + K_1(p_i - p_p) \\ \sigma_{\theta z} = G\sigma_h + H\sigma_H + J\sigma_v \\ \sigma_{r\theta} = \sigma_{rz} = 0 \end{cases} \tag{1}$$

where σ_r, σ_θ, σ_z, $\sigma_{r\theta}$, $\sigma_{\theta z}$, and σ_{rz} are the stress components of the wellbore in a cylindrical coordinate system as shown in Figure 2b, MPa; σ_v is the vertical stress, MPa; σ_H and σ_h are the maximum and minimum horizontal crustal stresses, respectively, MPa; p_i is BHP, MPa; p_p is the formation pressure, MPa; ϕ is the porosity of the formation; the undetermined coefficients A, B, C, D, E, F, D, H, I, J, and the coefficient related permeation K_1 are

$$\begin{cases} A = \cos\psi\left[\cos\psi(1 - 2\cos 2\theta)\sin^2\omega + 2\sin 2\omega \sin 2\theta\right] + (1 + 2\cos 2\theta)\cos^2\omega \\ B = \cos\psi\left[\cos\psi(1 - 2\cos 2\theta)\cos^2\omega - 2\sin 2\omega \sin 2\theta\right] + (1 + 2\cos 2\theta)\sin^2\omega \\ C = (1 - 2\cos 2\theta)\sin^2\psi \\ D = \sin^2\omega\sin^2\psi + 2\upsilon\sin 2\omega\cos\psi\sin 2\theta + 2\upsilon\cos 2\theta(\cos^2\omega - \sin^2\omega\cos^2\psi) \\ E = \cos^2\omega\sin^2\psi - 2\upsilon\sin 2\omega\cos\psi\sin 2\theta + 2\upsilon\cos 2\theta(\sin^2\omega - \cos^2\omega\cos^2\psi) \\ F = \cos^2\psi - 2\upsilon\sin^2\psi\cos 2\theta \\ G = -(\sin 2\omega\sin\psi\cos\theta + \sin^2\omega\sin 2\psi\sin\theta) \\ H = \sin 2\omega\sin\psi\cos\theta - \cos^2\omega\sin 2\psi\sin\theta \\ J = \sin 2\psi\sin\theta \\ K_1 = \frac{\alpha(1-2\upsilon)}{1-\upsilon} - \phi \end{cases} \tag{2}$$

where υ is Poisson's ratio; α is the Boit coefficient; ψ is the angle of inclination, °; ω is the angle from the direction of maximum horizontal stress to the projection line of well axis in Cartesian coordinates (x_1, y_1, z_1), °; θ is the angle from the x direction in the Cartesian coordinate to the direction of the radius vector, °.

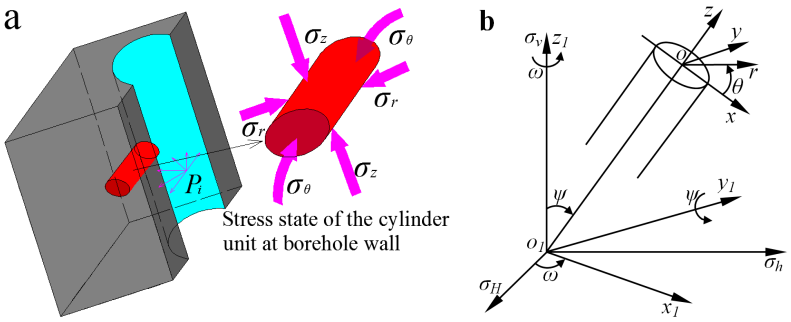

Figure 2. Stress state of the wellbore unit: (**a**) the formation unit; (**b**) the conversion of coordinates for an inclined wellbore.

The stress change from the conventional drilling method (OBD) to UBD means the decrease of BHP (P_i), and $0 < K_1 < 1$ resulting from α, υ, and ϕ of coal is a key condition to realize the change (see Table 2). The following conclusions can be inferred by Equation (1):

(1) Smaller radial stress (σ_r) corresponds to the lower BHP (P_i).
(2) Circular stress (σ_θ) increases with the decrease of BHP (P_i).

(3) Smaller axial stress (σ_z) corresponds to the lower BHP (P_i).

Therefore, different designs of BHP lead to various stress states of the wellbore, and the lower BHP results in higher deviatoric stress of the coal wellbore during UDB. The stress state of the cylinder unit at the borehole wall (Figure 2a) was simulated by the coal samples (Figure 3), which are reconstituted in the laboratory.

(1) An axial stress and a confining pressure are applied on a cylinder specimen, considering the stress of σ_θ and σ_r.
(2) Initial deviatoric stress of 8 MPa is applied on the specimens for simulating the difference of σ_θ and σ_r under the initial condition of OBD. Different degrees of UCP are used to simulate the different decrease levels of BHP.
(3) A gas pressure difference of 1.0 MPa is applied on the two ends of the specimens for simulating the field situation of the gas percolation gradient from the formation to the wellbore during UBD.

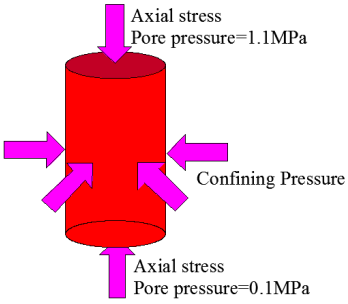

Figure 3. Stress state of a coal specimen.

This laboratory test considers three stress paths (Figure 4): unloading confining pressure (UCP) until coal failure is to evaluate the mechanical behavior and permeability of coal during pure UCP. Different degrees of UCP then reload the axial stress (RAS) tests until coal failure to measure the mechanical behavior and permeability of the coal under different designed BHP. The stress path of conventional triaxial compression (CTC) tests under different confining pressure is used for comparison. The experiment parameters are presented in Table 3.

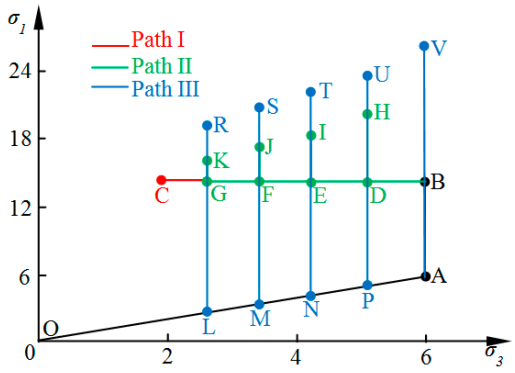

Figure 4. Stress paths of the tests.

Stress Path I (UCP test): Stage 1 (OA), an isotropic in situ stress state of $\sigma_{10} = \sigma_{30} = 6$ MPa is applied to the specimen. The methane tank connected to the specimen injects the methane into the specimen up to a gas pressure of 1.1 MPa. We close the gas outlet valve to maintain constant gas pressure. This state is maintained for 12 h to let the coal fully adsorb the methane under this pressure [4]. The gas

outlet valve is then opened and a differential gas pressure of 1 MPa is maintained at the two ends of the coal specimen. Stage 2 (AB), axial stress is loaded to 14 MPa given the confining pressure of 6 MPa for simulating the σ_θ and σ_r at the highest designed BHP. Stage 3 (BC), the axial stress remains constantly at 14 MPa and the confining pressure is decreased at an unloading rate of 0.02 MPa/s until coal specimen failure.

Table 3. Sample sizes and experimental parameters.

Sample	Stress Path	Length (mm)	Density (g/cm^3)	Confining Pressure (MPa)	Yield Deviatoric Stress (MPa)	Peak Deviatoric Stress (MPa)	At Peak Stress			Initial Permeability ($\times 10^{-17}$ m^2)
							ε_1 (%)	ε_3 (%)	ε_v (%)	
I-0	OABC	101.3	1.240	—	—	12.42	2.73	−1.64	−0.55	14.33
II-1	OABGK	98.4	1.252	2.6	—	12.42	3.08	−2.37	−1.66	13.76
II-2	OABFJ	102	1.219	3.72	—	14.00	3.77	−2.46	−1.15	14.48
II-3	OABEK	101.6	1.234	4.48	11.20	15.49	3.93	−2.53	−1.13	14.62
II-4	OABDH	98.8	1.253	5.24	13.98	16.88	4.02	−2.26	−0.17	14.57
III-0	OAV	102.8	1.229	6	18.29	22.67	4.27	−1.76	0.75	14.88
III-1	OLR	99.8	1.249	2.6	9.56	15.14	3.94	−3.50	−3.05	14.16
III-2	OMS	100.3	1.242	3.72	10.15	17.55	4.12	−2.79	−1.46	14.12
III-3	ONT	100.1	1.241	4.48	14.56	19.22	4.26	−2.33	−0.39	14.37
III-4	OPU	101.2	1.235	5.24	17.32	21.29	4.40	−2.34	−0.36	14.49

Stress Path II (UCP-RAS test): there are four stages for these tests. Stages 1 and 2 are the same as Stress Path I. Stage 3: UCP tests are conducted to the confining pressures of 5.24 MPa (D), 4.48 MPa (E), 3.72 MPa (F), and 2.6 MPa (G), respectively, with the unloading rate of 0.02 MPa/s. Stage 4: the axial stresses are continuously increased at a loading rate of 0.05 kN/s until the specimens fail under the current confining pressure.

Stress Path III (CTC test): these tests have two stages. Stage 1 is similar as the Stress Path I with the isotropic in situ stress state of 2.6 MPa (L), 3.72 MPa (M), 4.48 MPa (N), 5.24 MPa (P), and 6 MPa (A), respectively. Stage 2: the axial stress is continuously increased until these specimens fail under current confining pressure.

The whole experimental procedure is presented in Figure 5.

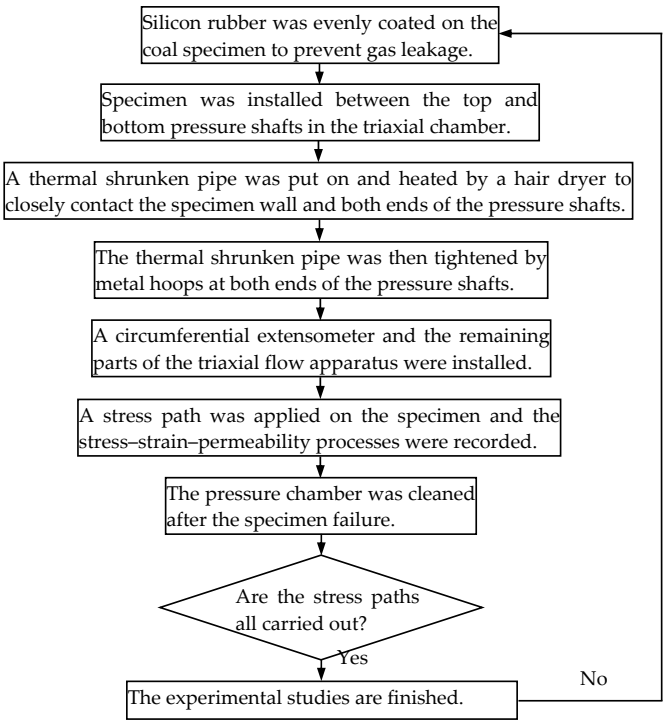

Figure 5. Experiment procedure of the tests.

3. Experimental Results and Analysis

The strains of coal specimens, including axial strain, radial strain, and volumetric strain, and the lateral expansion ratio are for evaluating the ductile deformation of coal under the stress path of UCP, UCP-RAS, and CTC tests. The deformation modulus is for analyzing the ability of resisting the deformation of coal. The peak deviatoric stress, cohesion, and internal friction angle are for estimation of the strength of coal.

3.1. Data Treatments

In the experiments, two lateral direction stresses are the same ($\sigma_2 = \sigma_3$), the volumetric strain can be calculated as

$$\varepsilon_V = \varepsilon_1 + 2\varepsilon_3 \tag{3}$$

where ε_V is volumetric strain, %; ε_1 is an axial strain, %; ε_3 is a radial strain.

Since coal is a nonlinear elastic material, the elastic modulus evolves with the deformation in the stress–strain process. For triaxial compression tests with UCP, deformation modulus E_0 and lateral expansion ratio μ_0 are defined as [11]

$$\begin{cases} \mu_0 = -\frac{\varepsilon_3}{\varepsilon_1} \\ E_0 = \frac{\sigma_1 - \sigma_3}{\varepsilon_1} \end{cases} \tag{4}$$

The methane gas permeation through the specimen is assumed to be isothermal and ideal. Thus, the permeability of coal can be calculated by [21,22]

$$K = \frac{2q\mu LP_2}{A\left(P_1^2 - P_2^2\right)} \tag{5}$$

where K is the permeability (m^2), q is the gas permeation rate (m^3/s), μ is the gas kinematic viscosity (Pas), L is the length of the coal specimens (m), S is the cross-sectional area of the coal specimens (m^2), P_1 is the gas pressure at the upper stream of specimens (Pa), and P_2 is the gas pressure downstream of the specimens (Pa).

3.2. UCP and CTC Affecting the Mechanical Behavior and Permeability

Figure 6 presents the stress–strain process of coal I-0 and III-0. In Figure 6a, the stress–strain curves of coal I-0 and III-0 at Stage 2 have a high uniformity. Until Stage 3, the peak of deviatoric stress (coal I-0) reduces compared to the peak of deviatoric stress (coal III-0). This reveals damage due to unloading confining pressure is more obvious, leading the coal specimen to be prone to failure. In addition, the UCP test has no elastic deformation stage. After starting the UCP, the deviatoric stress-axial strain curve is protruding and its yield point is not clear. At the point of the coal failure, the UCP test has lower axial strain (Figure 6a) and volumetric strain than the CTC test (Figure 6b). The radial strain of the UCP test is similar with that of the CTC test (Figure 6c). The larger radial strain of coal during unloading confining pressure (Figure 6c) causes more damage and larger volume expansion (Figure 6b). This may lead the poorer mechanical strength and the lower ability for ductile deformation of the coal specimen of UCP.

Figure 7 presents the change of deformation modulus and lateral expansion ratio of coal I-0 and III-0. In Stage 3, the deformation modulus reduces 64.95% for coal I-0 and 28.47% for coal III-0. Amplification of the lateral expansion ratio increases 311.48% for coal I-0 and 204.70% for coal III-0. The lateral expansion ratio of coal I-0 is larger than 0.5. The mechanical strength and the ability of ductile deformation of coal under the UCP test could decrease.

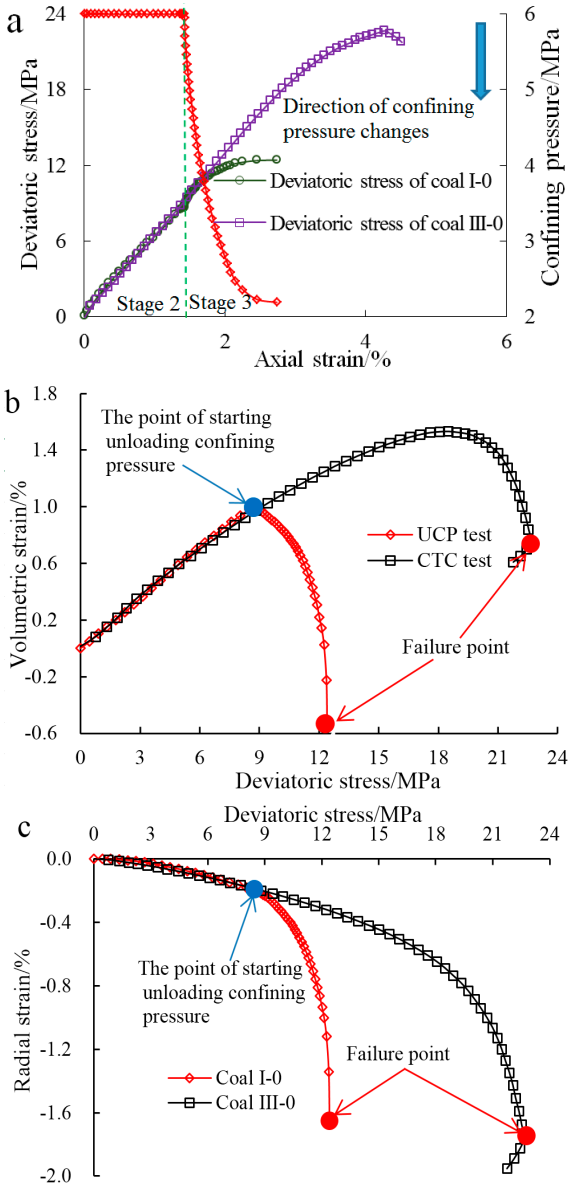

Figure 6. Stress–strain process of coal I-0 and coal III-0 (Stage 2 and Stage 3 in reference to Stress Path II): (**a**) stress vs. axial strain; (**b**) stress vs. volumetric strain; (**c**) stress vs. radial strain.

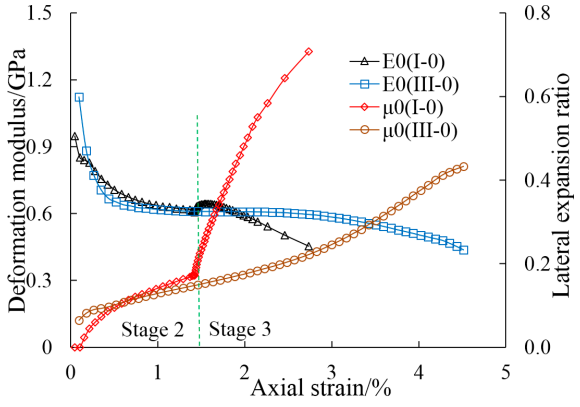

Figure 7. Change of the deformation modulus and lateral expansion ratio of coal I-0 and III-0 (Stage 2 and Stage 3 in reference to Stress Path II).

Permeability evolutions of coal I-0 and III-0 are as shown in Figure 8. In Stage 3, the permeability of coal I-0 increases immediately, while III-0 has a long time lag for the increase, as shown in Figure 8a. In Figure 8b, the permeability evolution of coal I-0 with the volumetric strain indicates higher volumetric strain corresponding to lower permeability, while the permeability of coal III-0 increases when the moment of decreasing volumetric strain reaches that of coal failure. These phenomena are due to the more rapid radial deformation of I-0 than that of III-0 (Figure 6c), producing more fractures along the radial direction [4].

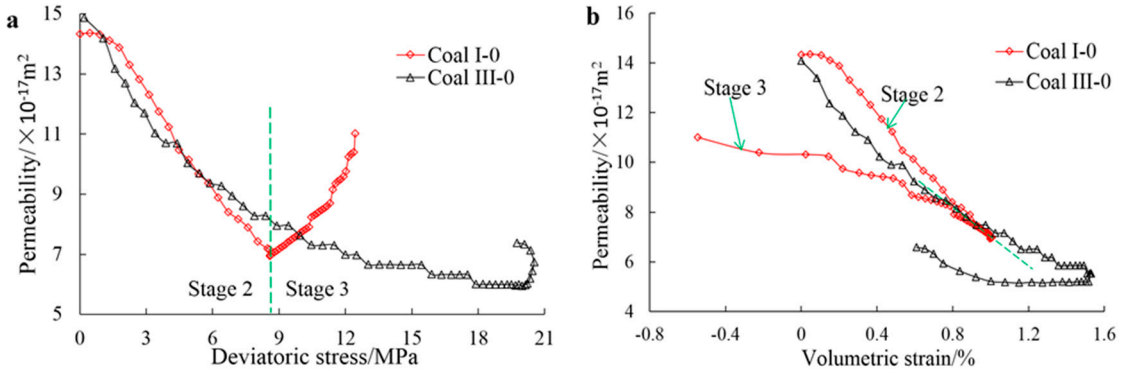

Figure 8. Permeability evolution of coal I-0 and III-0 (Stage 2 and Stage 3 with reference to Stress Path II): (**a**) permeability-deviatoric stress curve; (**b**) permeability-volumetric strain curve.

3.3. Mechanical Behavior and Permeability of Coal Rock under Different Degrees of UCP-RAS Test

3.3.1. Stress–Strain of Coal Rock

Figure 9 presents the stress–strain process of coals for coal II-1, II-2, II-3, II-4, and for coal III-1, III-2, III-3, and III-4. Firstly, the peak strengths under UCP-RAS tests are lower than these under CTC tests, as shown in Figure 10a. Secondly, the yield deviatoric stresses of coal II-3 and II-4 are lower by 23.08% and 19.28% than these of coal III-3 and III-4, respectively. The coal II-1 and II-2 have no elastic deformation during Stages 3 and 4. These phenomena mean that the elastic deformation of coal after suffering UCP becomes short. Thirdly, coal samples under UCP-RAS tests have larger volume expansion than those under CTC tests. All of the volumetric strains of coal specimens after suffering CUP decrease with the increase of deviatoric stress at Stage 4. Differently, the decreases of coal specimens under CTC tests appear after the yield point. Fourthly, coal specimens under UCP-RAS tests have lower ductile deformation than those under CTC tests. This evidence mean that the process of UCP tests damages coal, and a higher degree of UCP has a lower mechanical behavior. Figure 10a indicates the damage degree of the peak strength of coal linearly relates the current confining pressure by unloading of UCP-RAS. Figure 10b shows the linear relation between the reduction of confining pressure by UCP and the peak strength of coal.

3.3.2. Deformation Modulus and Lateral Expansion Ratio of Coal

Figure 11 presents the relationships of the deformation modulus and lateral expansion ratio with the axial strain for coal II-1, II-2, II-3, II-4, and for coal III-1, III-2, III-3, and III-4. In Figure 11a, firstly, the deformation modulus of coal II-1, II-2, II-3, and II-4 is lower than those of coal III-1, III-2, III-3, and III-4, respectively, at Stage 4. With the axial strain increasing from 2.45% to 3.39%, the deformation moduli under the CTC test decrease by 16.52%, 13.51%, 7.96%, and 1.17% for coal III-1, III-2, III-3, and III-4, respectively. Correspondingly, the deformation moduli under the RAS test decreases by 23.80%, 18.11%, 15.84%, and 12.06% for coal II-1, II-2, II-3, and II-4, respectively. The decrease of the deformation modulus of coal during the RAS test is more significant than that during the CTC test and the higher degree of UCP has a larger decrease of deformation modulus. Figure 11b shows that the

lateral expansion ratios of coal under the RAS test are larger than those under the CTC test under the same confining pressure and axial strain. All of this indicates that coal, after suffering the UCP test, presents a lower ability of ductile deformation compared to the coal after suffering the CTC test.

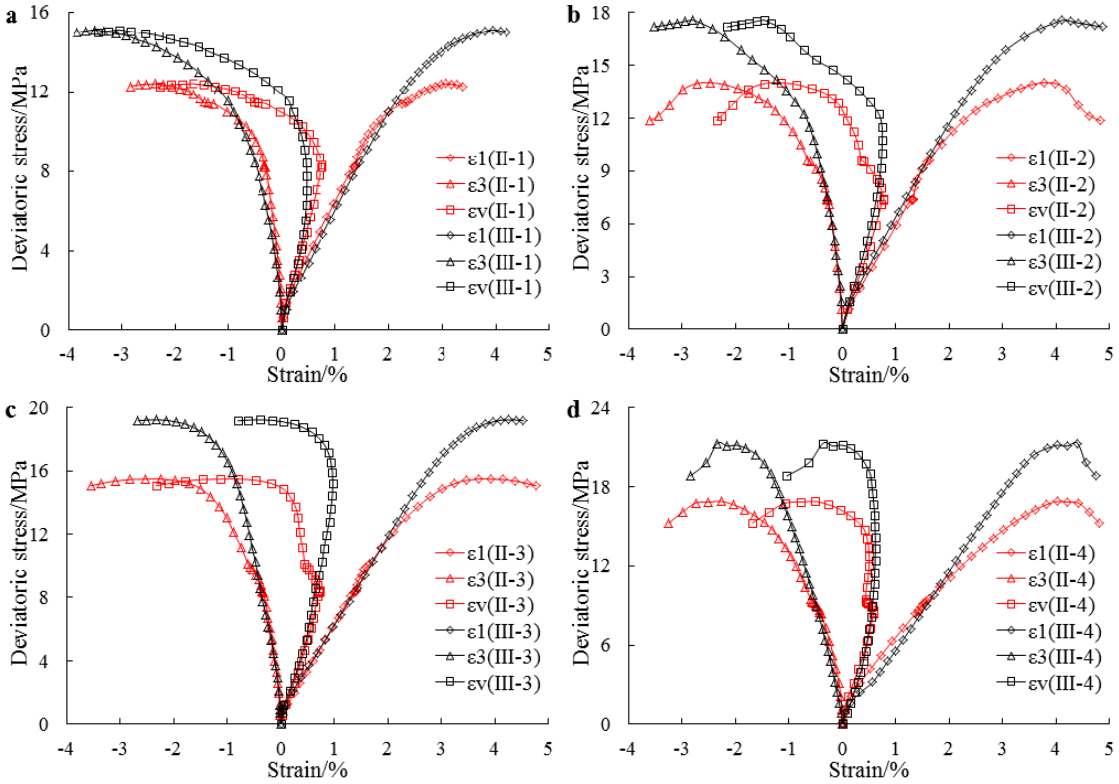

Figure 9. Stress–strain of the coal specimens: (**a**) for coal II-1 and III-1; (**b**) for coal II-2 and III-2; (**c**) for coal II-3 and III-3; (**d**) for coal II-4 and III-4.

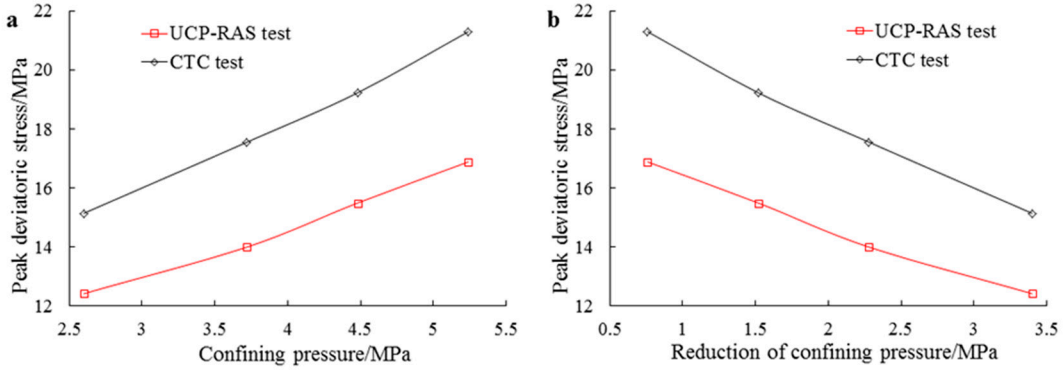

Figure 10. Unloading confining pressure damaging the peak strength of coal for UCP-RAS and CTC tests. (**a**) Peak deviatoric stress vs. current confining pressure; (**b**) peak deviatoric stress vs. reduction of confining pressure.

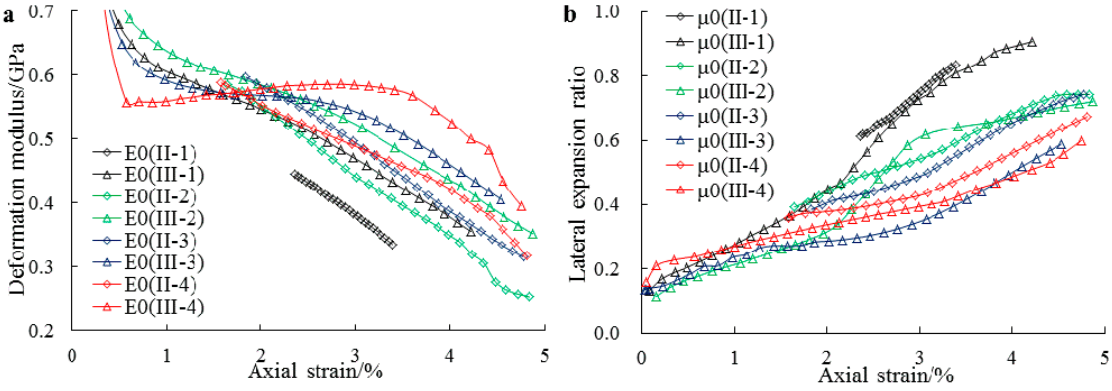

Figure 11. Change of deformation modulus (**a**) and lateral expansion ratio (**b**) with the axial strain.

3.3.3. Permeability Evolutions of the Coal Rock

Figure 12 presents the permeability evolution of coal for coal II-1, II-2, II-3, II-4, and for coal III-1, III-2, III-3, and III-4. Firstly, the permeability of coal II-1, II-2, II-3, and II-4 decrease faster than those of coal III-1, III-2, III-3, and III-4, respectively, during Stage 2. This may be due to the confining pressure of the UCP-RAS test being higher than that of the CTC test during Stage 2. Secondly, permeability under UCP-RAS tests increase immediately when Stage 3 starts, while the permeability under the CTC tests increases near the peak strength. Thirdly, the higher degree of UCP has a larger increase of permeability during Stage 3. Fourthly, permeability under the UCP-RAS test during Stage 4 increases faster than those under the CTC test.

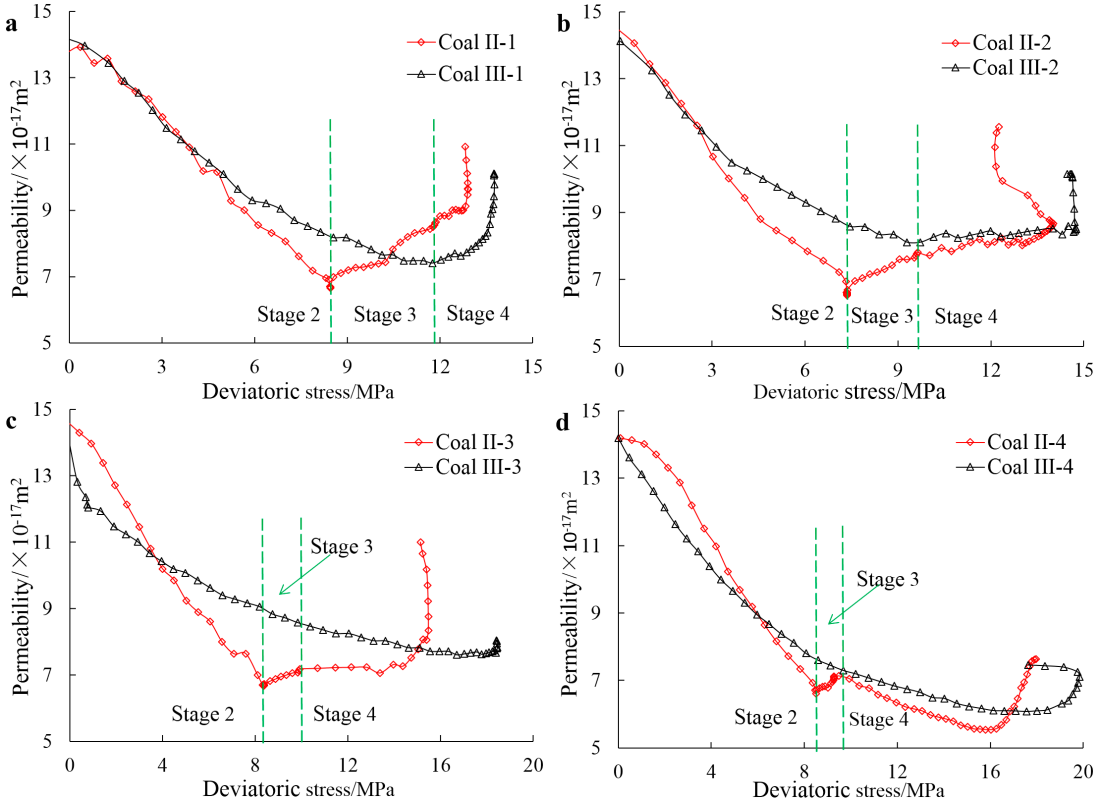

Figure 12. Permeability evolution with deviatoric stress: (**a**) for coal II-1 and III-1; (**b**) for coal II-2 and III-2; (**c**) for coal II-3 and III-3; (**d**) for coal II-4 and III-4 (Stage 2, Stage 3, and Stage 4 with reference to Stress Path II).

3.4. Cohesion and Friction Angle Calculated by the UCP-RAS Test

Figure 13 presents the Mohr's stress circle under the CTC test and UCP-RAS test. The results show that both coal specimens under the CTC test and UCP-RAS test agree well with the Mohr-Coulomb failure criterion. The cohesion and internal friction angle were calculated by fitting the peak strength Mohr's circles under four different confining pressures. The results show that the cohesion and internal friction angle calculated by UCP-RAS are lower at 4.57% and 15.18% than that calculated by the CTC test. This indicates that the strength parameters of coal after suffering UCP have been reduced, especially the internal friction angle.

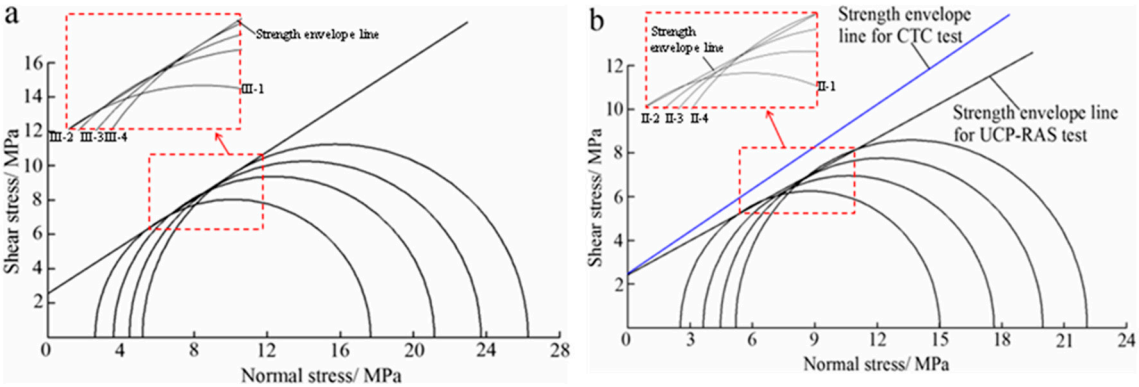

Figure 13. Mohr's stress circle of coal specimens: (**a**) under the CTC test; (**b**) under the UCP-RAS test.

3.5. Error Analysis of Experiments

On one hand, the stress–strain curves of coal I-0 and coal III-0 during Stage 2 (elastic deformation stage) are consistent with relative average deviations of elasticity modulus of 4.01% (Figure 6) indicating high replication of the stress–strain of the coal. On the other hand, at the initial hydrostatic pressure state, the permeability of all coal specimens are from 13.76×10^{-17} to 14.88×10^{-17} m^2 showing the coal specimens' high consistency with relative average deviations of 1.60% (Table 3). The better fitting degree of the Mohr's stress circle under the CTC and UCP-RAS tests can also verify the reliability of the results. The measuring errors of the experimental apparatus are <0.1% for stress, strain, and permeability (Table 1) and the relative average deviations of the material properties of coal blocks (raw coal) are 1.61% for density, 6.31% for BET surface area, 11.99% for porosity, 21.29% for elasticity modulus, 12.66% for Poisson's ratio, and 9.72% for Boit coefficient (Table 2). Therefore, it can be inferred that the reconstituted coal specimen from the coal blocks has much smaller relative average deviation (for example, 0.66% for density in Table 3). Generally, both the equipment error and material error do not affect the reliability of the research results significantly.

4. A Field Case of the Well Collapse Problem during the Process from OBD to UBD

A horizontal test well with a potential well collapse problem lies in the Zhaozhuang well field in the southeast slope area of the Qinshui Basin, China (Figure 14). The formation in Zhaozhuang is a structure with the dip angle of 5°–10°, with a NW dip direction. Moreover, there are some wide and gentle folds and fault structures resulting in the significant development of joints. The CBM reservoir, whose thickness is 0.79–6.6 m with an average value of 4.53 m, lies in the third coal seam of Zhaozhuang. Its depth is 612.62–768.63 m with an average value of 685.07 m. Its gas content is 10.14–21.82 m^3/t with an average value of 15.88 m^3/t [23]. The in situ stress field mainly contributed by tectonic stress is dominated by horizontal stress.

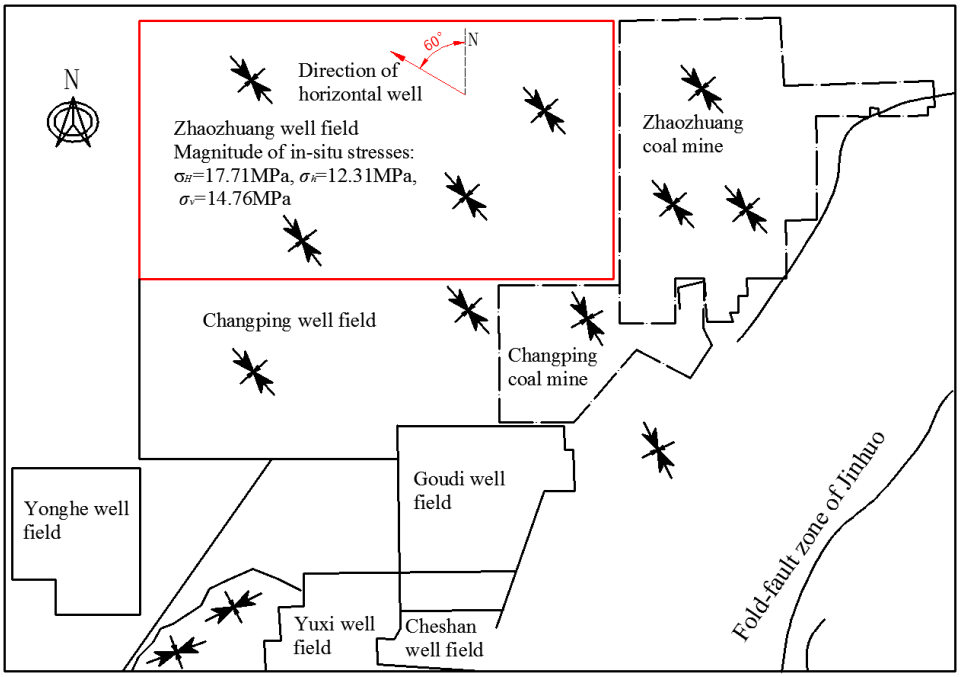

Figure 14. In situ stress distribution map of the Zhaozhuang well field (modified after [24] with permission from Kang et al., 2009).

This horizontal test well has a well depth of 1993.24 m and vertical depth of 720 m. The inclined direction of the wellbore is N60°W. OBD with a fluid density of 1.6 g/cm^3 was used for drilling the vertical well and kick-off sections. UBD was designed to drill the horizontal section for avoiding reservoir pollution.

Table 4 lists the formation parameters of this research area and the rock mechanical properties tested in our experiments. The formation parameters come from the well log analysis of this horizontal test well. The Poisson ratio and Biot coefficient are the average values of the tests, respectively. It is suspected that an increase of deviatoric stress caused by the decrease of the strength of the coal wellbore due to the UCP squeezes the drill fluid. In order to be against this increase of deviatoric stress, an object of higher drilling fluid density should be designed. For this case, based on the formation condition and rock mechanical properties by CTC testing, the drilling fluid density designed by the method from Ma et al. [25] and Ma and Chen [26] must be larger than 1.017 g/cm^3 to avoid wellbore collapse (Figure 15). In real scenarios, the decrease of drilling fluid density was much faster than expected. The field monitoring revealed that the total hydrocarbon content increased significantly when the drilling fluid density reduced to 1.103 g/cm^3. This phenomenon indicated that the gas flowed into the wellbore at that moment [27] and may be caused by the failure of coal surrounding the wellbore under the condition of unloading confining pressure as presented in Section 3.3.3. In addition, when the drilling fluid density decreased to 1.103 g/cm^3, wellbore collapse appeared and the lower drilling fluid density led to higher hydrocarbon content and more serious wellbore collapse. While using the formation condition and rock mechanical properties from the UCP-RAS test, the drilling fluid density should be greater than 1.176 g/cm^3 (Figure 15) for maintaining the stability of the well. Therefore, designing a drilling fluid density of 1.05 g/cm^3 based on CTC for UBD is likely underestimated.

Table 4. Formation and rock parameters of the third coal seam.

Formation Parameters						
Vertical depth (m)	Formation pressure gradient (MPa/100 m)	Gradient of maximum horizontal in-situ stress (MPa/100 m)	Gradient of minimum horizontal in-situ stress (MPa/100 m)	Gradient of vertical stress (MPa/100 m)	Azimuthal angle of maximum horizontal stress (°)	Porosity (%)
720	1.109	2.46	1.71	2.05	N30W	0.1

Rock parameters							
CTC				UCP-RAS			
Poisson ratio	Biot coefficient	Cohesion (MPa)	Internal friction angle (°)	Poisson ratio	Biot coefficient	Cohesion (MPa)	Internal friction angle (°)
0.271	0.476	2.494	32.340	0.365	0.532	2.380	27.431

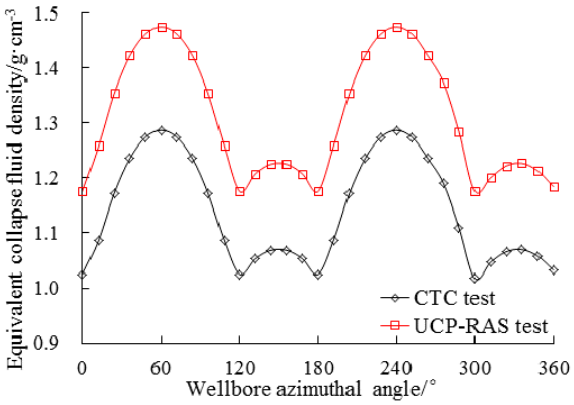

Figure 15. Equivalent collapse fluid density (minimum drilling fluid density for well stability) considering the wellbore azimuthal angle of the horizontal well.

5. Discussion

5.1. The Effect of the UCP Test on the Mechanical Behavior and Permeability of Coal

Unloading confining pressure damages the rock materials to some extent [4]. Figure 16 presents the Mohr's circles of coal in Stress Paths II and III. For the stress state of Stress Circle S2, the axial stress increases from hydrostatic pressure of σ_3 to σ_1 and the confining pressure decreases from σ_3 to σ'_3 under Stress Path II while Stress Path II is a simple increase of axial stress from σ'_3 to σ_1. Figure 17 presents the strain of coal specimens at the stress state of Stress Circle S2. It is clearly seen that the strains of the coal specimens under Stress Path II are all greater than these under Stress Path III. This may be due to the vertical fractures being more sensitive to the confining pressure. UCP can lead to the production of a sharp increase of radial strain, resulting in untightening of the pores, voids, and fractures along the vertical direction under an initial deviatoric stress.

This untightening of the pores, voids, and fractures is an inelastic, unrecoverable deformation. The inelastic extension of the radial direction of the coal specimen can reduce the mechanical strength [4]. Therefore, the coal specimens, after suffering the UCP test, could be easily damaged during the RAS test, resulting in the decrease of cohesion and internal friction angle (Section 3.4) and an increase of Poisson ratio (Figure 11). In addition, the pores, voids, and fractures increased, enlarging the permeability of the coal. This reduces the resistant force against the gas seepage in the downstream section of the coal specimen leading the increases of gas pressure in the whole coal specimen. This high gas pressure can accelerate the failure of coal [28].

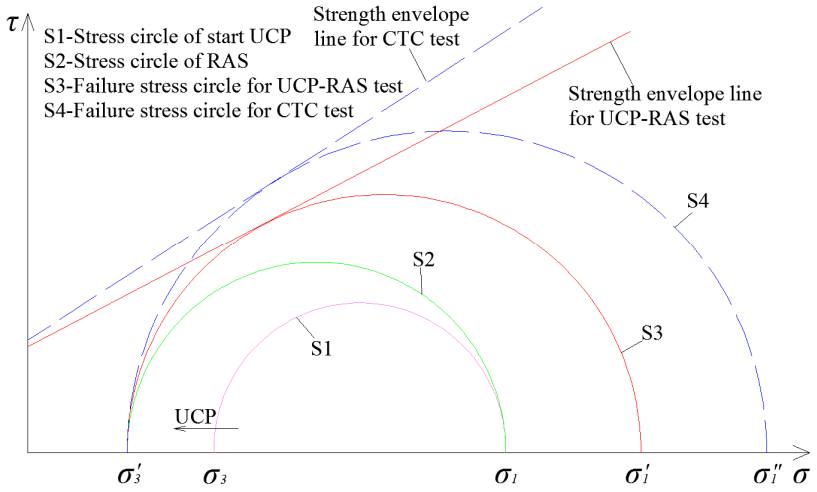

Figure 16. Mohr's circles of coal in Stress Paths II and III.

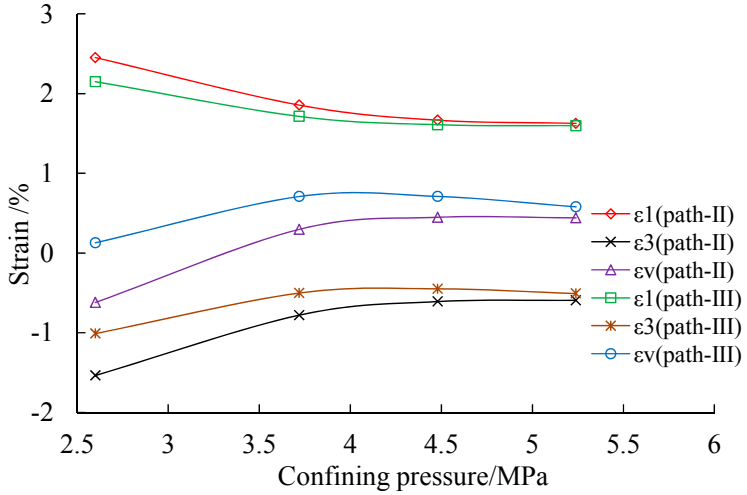

Figure 17. Strain of coal specimens under the stress state of Stress Circle S1.

5.2. The Field Application of CTC and UCP-RAS Tests during UBD

UBD usually drills the CBM reservoir to protecting the reservoir from drilling fluid pollution [29]. During the procedure of UBD, the BHP should decrease to a designed value that is lower than the formation pressure [2]. Thus, unloading confining pressure (UCP) is a very common phenomenon during UBD. It suspected that an increase of deviatoric stress caused by the decrease of the strength of the coal wellbore due to the UCP squeezes the drilling fluid [30], since the decrease of BHP is similar to UCP [31]. The strength parameters using the CTC test are overestimated due to not considering the coal damage from UCP. Thus, the case of the Zhaozhuang well field (Figure 14) shows the strength parameters using the CTC test could underestimate the probability of well collapse during UBD. In addition, during UBD, the gas flows from the reservoir into the wellbore result in further reducing BHP [27]. As a result, the UCP-RAS, rather than the CTC test, can better reflect the strength parameters during UBD. On the other hand, UCP has a positive effect for increasing the permeability of coal. It is beneficial to improve the reservoir connectivity and the CBM production.

5.3. Usage of Reconstituted Coal Specimens and Their Application in the Field

In this case, the high difference in maximum horizontal in situ stress and minimum horizontal in situ stress of 5.4 MPa (Figure 14) caused rich microfractures resulting in soft and fragile coal

blocks of the third coal seam. It is not easy to collect an intact coal block for preparing a raw coal specimen. Additionally, the difference of test data of reconstituted coal and raw coal is not significant; for example, deviation of reconstituted coal is 4.23% for Poisson's ratio and 10.19% for the Boit coefficient compared to the values of raw coal calculated by the data in Tables 2 and 4. In addition, the references of Liu et al. [32] and Jasinge et al. [33] indicated most variation tendencies of the physical properties of reconstituted coal and raw coal were consistent. Other aspects, such as the highly heterogeneous nature of coal, sometimes makes it difficult to interpret the results of laboratory experiments. Due to the heterogeneity of natural materials property, calculation and measurement of parameters are not often precise. This makes it difficult to characterize and understand the coal properties for developing ideal models for optimization of sequestration processes and generating useful correlations [34]. More homogeneous samples with properties reproducible in the laboratory would provide significant advantages, especially in understanding the effects of various factors in the properties of coal [35–38]. Therefore, in this study, reconstituted coal specimens were used in the laboratory experiments. It should be known that the results obtained by the reconstituted coal specimens, although having the advantage of good regularity to investigate the effect of UCP on the mechanical behavior and permeability during reloading axial stress, do not accurately represent the actual mechanical behavior of the in situ coal field. However, to some extent, the results can reflect the universal law from the perspective of engineering practice. It has some value in application of coalbed methane drilling engineering. We also have to point out this study mainly focuses on the soft rocks, like coal, whose mechanical behavior and permeability are sensitive to the UCP. Since coal under different UCP shows non-uniform damage, the cohesion and friction angle of coal specimens may not be calculated by the Mohr-Coulomb failure criterion very precisely.

6. Conclusions

A series of experimental studies were conducted to measure the mechanical behavior and gas permeability of coal in CTC and UCP-RAS tests. We also discussed the cause of overestimation of coal wellbore stability using the CTC test. Based on these results, several conclusions can be drawn.

Firstly, the mechanical behavior of coal under the UCP-RAS test is lower than that under the CTC test, including (1) the peak deviatoric stress of coal by UCP-RAS is much smaller; (2) the coal suffering the UCP test has a shorter elastic deformation and a higher UCP degree, leading to an inelastic deformation; (3) the deformation modulus of coal by UCP-RAS reduces faster; (4) during the UCP test the coal has a higher lateral expansion ratio; (5) both the cohesion and internal friction angle of coal under the UCP-RAS test are lower.

Secondly, under the UCP-RAS test the permeability of coal increases immediately when the confining pressure reduces, and the higher degree of UCP has a larger increase of permeability. The permeability of coal suffering the UCP test increases faster and the higher UCP degree leads to a faster increase of permeability during the RAS test.

Finally, a significant increase of equivalent collapse density was calculated by using the rock parameters of the UCP-RAS test. Thus, during UBD measuring the rock mechanical parameters could come from the UCP-RAS test rather than the CTC test.

Acknowledgments: The financial support obtained from the National Natural Science Foundation of China (Grant No. 51474185), Scientific Research Foundation of State Key Lab. of Coal Mine Disaster Dynamics and Control (2011DA105287-FW201203), the China Postdoctoral Science Foundation (Grant No. 2014M560728), and the Young Scholars Development Fund of SWPU (Grant No. 201231010031) is appreciated.

Author Contributions: Drafting of manuscript: Wen Nie and Qiangui Zhang; acquisition of data: Yongchang Liang and Minghui Li; analysis and interpretation of data: Qiangui Zhang and Wen Nie; Model in the case: Tianshou Ma; Real measurement data in the case: Guangzhi Li, and planning and supervision of the research: Xiangyu Fan.

Conflicts of Interest: The authors declare no conflict of interest.

Abbreviations

The following abbreviations are used in this manuscript:

σ_r	radial stress at the wellbore in cylindrical coordinate system, MPa
σ_θ	circumferential stress at the wellbore in cylindrical coordinate system, MPa
σ_z	axial stress at the wellbore in cylindrical coordinate system, MPa
$\sigma_{r\theta}$	stress in r-θ plane at the wellbore in cylindrical coordinate system, MPa
$\sigma_{\theta z}$	stress in θ-z plane at the wellbore in cylindrical coordinate system, MPa
σ_{rz}	stress in r-z plane at the wellbore in cylindrical coordinate system, MPa
σ_v	vertical stress, MPa
σ_H	maximum horizontal in-situ stress, MPa
σ_h	minimum horizontal in-situ stress, MPa
p_i	bottle hole pressure (BHP), MPa
p_p	formation pressure, MPa
ϕ	porosity of the formation, 1
υ	Poisson's ratio, 1
α	boit coefficient, 1
ψ	angle of inclination, $^\circ$
ω	angle from the direction of maximum horizontal stress to the projection line of well axis into the Cartesian coordinate (x_1, y_1, z_1), $^\circ$
θ	the angle from the x direction in the Carteesian coordinate to the direction of radius vector, $^\circ$
K	permeability, m^2
q	gas permeation rate, m^3/s
μ	gas kinematic viscosity, Pas
L	length of the coal specimens, m
S	cross-sectional area of the coal specimens, m^2
P_1	gas pressure at the upper stream of specimens, Pa
P_2	gas pressure at the downstream of the specimens, Pa
ε_1	axial strain, %
ε_3	radial strain, %
ε_V	the volumetric strain, %
σ_1	the axial stress on coal speicmen, MPa
σ_3	the radial stress on coal speicmen, MPa
E_0	deformation modulus, GPa
μ_0	lateral expansion ratio, 1
K_1	the coefficient related permeation, 1
A, B, C, D, E, F, D, H, I, J	undetermined coefficients, 1

References

1. Tian, L.; Cao, Y.; Chai, X.; Liu, T.; Feng, P.; Feng, H.; Zhou, D.; Shi, B.; Oestreich, R.; Rodvelt, G. Best practices for the determination of low-pressure/permeability coalbed methane reservoirs, Yuwu Coal Mine, Luan mining area, China. *Fuel* **2015**, *160*, 100–107. [CrossRef]
2. He, S.; Wang, W.; Shen, H.; Tang, M.; Liang, H.; Lu, J. Factors influencing wellbore stability during underbalanced drilling of horizontal wells-When fluid seepage is considered. *J. Nat. Gas Sci. Eng.* **2015**, *23*, 80–89. [CrossRef]
3. Kaffash, A.; Zare-Reisabadi, M.R. Borehole stability evaluation in overbalanced and underbalanced drilling: Based on 3D failure criteria. *Geosyst. Eng.* **2013**, *16*, 175–182. [CrossRef]
4. Yin, G.; Li, M.; Wang, J.; Xu, J.; Li, W. Mechanical behavior and permeability evolution of gas infiltrated coals during protective layer mining. *Int. J. Rock Mech. Min. Sci.* **2015**, *80*, 292–301. [CrossRef]

5. Fan, X.; Zhang, Q.; Wang, J.; Xu, L.; Zhang, P.; Jia, W.; Chen, X.; Yu, G.; Yang, Y. Mathematical methods for evaluating a reservoir based on gas dynamic monitoring during underbalanced drilling. *J. Nat. Gas Sci. Eng.* **2015**, *26*, 1068–1079. [CrossRef]
6. Zhang, Q.; Fan, X.; Chen, P.; Li, G.; Li, M.; Ma, T. Experimental study on gas flow and mechanical behaviors of coalbed near borehole under constant flow and CBM pressures. *J. China Univ. Pet.* **2015**, *39*, 94–101. (In Chinese)
7. Deisman, N.; Gentzis, T.; Chalaturnyk, R.J. Unconventional geomechanical testing on coal for coalbed reservoir well design: The Alberta Foothills and Plains. *Int. J. Coal Geol.* **2008**, *75*, 15–26. [CrossRef]
8. Iwata, N.; Sasaki, T.; Yoshinaka, R.; Kurooka, K. Applicability of the multiple yield model for estimating the deformation of vertical rock walls during large-scale excavations. *Int. J. Rock Mech. Min. Sci.* **2012**, *52*, 171–180. [CrossRef]
9. Qiu, S.; Feng, X.; Xiao, J.; Zhang, C. An Experimental study on the pre-peak unloading damage evolution of marble. *Rock Mech. Rock Eng.* **2014**, *47*, 401–419. [CrossRef]
10. Xie, H.; He, C. Study of the unloading characteristics of a rock mass using the triaxial test and damage mechanics. *Int. J. Rock Mech. Min. Sci.* **2004**, *41*, 74–80. [CrossRef]
11. Yin, G.; Jiang, C.; Wang, J.; Xu, J. Geomechanical and flow properties of coal from loading axial stress and unloading confining pressure tests. *Int. J. Rock Mech. Min. Sci.* **2015**, *76*, 155–161. [CrossRef]
12. Huang, D.; Li, Y. Conversion of strain energy in triaxial unloading tests on marble. *Int. J. Rock Mech. Min. Sci.* **2014**, *66*, 160–168. [CrossRef]
13. Yin, G.; Li, W.; Jiang, C.; Li, M.; Li, X.; Liu, H.; Zhang, Q. Mechanical property and permeability of raw coal containing methane under unloading confining pressure. *Int. J. Min. Sci. Technol.* **2013**, *23*, 789–793. [CrossRef]
14. Chen, H.; Cheng, Y.; Zhou, H.; Li, W. Damage and permeability development in coal during unloading. *Rock Mech. Rock Eng.* **2013**, *46*, 1377–1390. [CrossRef]
15. Meng, L.; Li, T. Experimental study on the permeability of phyllite under unloading confining pressure and high temperature. *Disaster Adv.* **2013**, *6*, 31–38.
16. Chen, H.; Cheng, Y.; Ren, T.; Zhou, H.; Liu, Q. Permeability distribution characteristics of protected coal seams during unloading of the coal body. *Int. J. Rock Mech. Min. Sci.* **2014**, *71*, 105–116. [CrossRef]
17. Meng, L.; Li, T.; Xu, J.; Chen, G.; Ma, H.; Yin, H. Deformation and failure mechanism of phyllite under the effects of THM coupling and unloading. *J. Mt. Sci.* **2012**, *9*, 788–797. [CrossRef]
18. Yin, G.; Jiang, C.; Wang, J.; Xu, J. Combined effect of stress, pore pressure and temperature on methane permeability in anthracite coal: An experimental study. *Transp. Porous Media* **2013**, *100*, 1–16. [CrossRef]
19. Tao, Y.; Liu, D.; Xu, J.; Peng, S.; Nie, W. Investigation of the Klinkenberg effect on gas flow in coal matrices: A numerical study. *J. Nat. Gas Sci. Eng.* **2016**, *30*, 237–247. [CrossRef]
20. Chen, M.; Jin, Y.; Zhang, G. *Rock Mechanics Relating to Petroleum Engineering*; Science Press: Beijing, China, 2008; pp. 59–60. (In Chinese)
21. Vishal, V.; Ranjith, P.G.; Pradhan, S.P.; Singh, T.N. Permeability of sub-critical carbon dioxide in naturally fractured Indian bituminous coal at arrange of down-hole stress conditions. *Eng. Geol.* **2013**, *167*, 148–156. [CrossRef]
22. Vishal, V.; Singh, T.N. A laboratory investigation of permeability of coal to supercritical CO_2. *Geotech. Geol. Eng.* **2015**, *33*, 1009–1016. [CrossRef]
23. Wang, Y. Geological factor of the coal-bad methane well in Zhaozhuang well field in the Qinshui Basin, China. *Coal* **2012**, *21*, 59–60. (In Chinese)
24. Kang, H.; Jiang, T.; Zhang, X.; Yan, L. Research on in-situ stress field in Jincheng mining area and its application. *Chin. J. Rock Mech. Eng.* **2009**, *28*, 1–8. (In Chinese)
25. Ma, T.; Chen, P.; Yang, C.; Zhao, J. Wellbore stability analysis and well path optimization based on the breakout width model and Mogi-Coulomb criterion. *J. Pet. Sci. Eng.* **2015**, *135*, 678–701. [CrossRef]
26. Ma, T.; Chen, P. A wellbore stability analysis model with chemical-mechanical coupling for shale gas reservoirs. *J. Nat. Gas Sci. Eng.* **2015**, *26*, 72–98. [CrossRef]
27. Fan, X.; Wang, J.; Zhang, Q.; Zhou, X.; Yu, G. An evaluation of porosity and permeability based on an unsteady seepage model in a reservoir while underbalanced drilling. *J. Pet. Sci. Eng.* **2015**, *127*, 367–376. [CrossRef]

28. Nie, W.; Peng, S.; Xu, J.; Liu, L.; Wang, G.; Geng, J. Experimental analyses of the major parameters affecting the intensity of outbursts of coal and gas. *Sci. World J.* **2014**, *2014*, 185608.
29. Lim, S.N.; Khalil, M.; Jan, B.M.; Ali, B.S. Lightweight biopolymer drilling fluid for underbalanced drilling: An optimization study. *J. Pet. Sci. Eng.* **2015**, *129*, 178–188. [CrossRef]
30. Gentzis, T.; Deisman, N.; Chalaturnyk, R.J. A method to predict geomechanical properties and model well stability in horizontal boreholes. *Int. J. Coal Geol.* **2009**, *78*, 149–160. [CrossRef]
31. He, S.; Wang, W.; Tang, M.; Hu, B.; Xue, W. Effects of fluid seepage on wellbore stability of horizontal wells drilled underbalanced. *J. Nat. Gas Sci. Eng.* **2014**, *21*, 338–347. [CrossRef]
32. Liu, Q.; Cheng, Y.; Ren, T.; Jing, H.; Tu, Q.; Dong, J. Experimental observations of matrix swelling area propagation on permeability evolution using natural and reconstituted samples. *J. Nat. Gas Sci. Eng.* **2016**, *34*, 680–688. [CrossRef]
33. Jasinge, D.; Ranjith, P.G.; Choi, X.; Fernando, J. Investigation of the influence of coal swelling on permeability characteristics using natural brown coal and reconstituted brown coal specimens. *Energy* **2012**, *39*, 303–309. [CrossRef]
34. Vishal, V.; Ranjith, P.G.; Singh, T.N. Geomechanical attributes of reconstituted indian coals under carbon dioxide saturation. In *Rock Mechanics for Resources, Energy and Environment*; CRC Press: Boca Raton, FL, USA, 2013; pp. 171–173.
35. Jasinge, D.; Ranjith, P.G.; Choi, S.K.; Kodikara, J.; Arthur, M.; Li, H. Mechanical properties of reconstituted Australian black coal. *J. Geotech. Geoenviron. Eng.* **2009**, *135*, 980–985. [CrossRef]
36. Ranjith, P.G.; Jasinge, D.; Choi, S.K.; Mehic, M.; Shannon, B. The effect of CO_2 saturation on mechanical properties of Australian black coal using acoustic emission. *Fuel* **2010**, *89*, 2110–2117. [CrossRef]
37. Jasinge, D.; Ranjith, P.G.; Choi, S.K. Development of a reconstituted brown coal material using cement as a binder. *Environ. Earth Sci.* **2011**, *64*, 631–641. [CrossRef]
38. Ranjith, P.G.; Shao, S.S.; Jaysinge, D.R. V.D. Carbon dioxide storage in coal-reconstituted coal as a structurally homogeneous substitute for coal. *Int. J. Coal Prep. Util.* **2012**, *32*, 265–275.